Protective effects of astaxanthin on particulate matter 2.5-induced senescence in HaCaT keratinocytes via maintenance of redox homeostasis

AO XUAN ZHEN*, KYOUNG AH KANG*, MEI JING PIAO, PINCHA DEVAGE SAMEERA MADUSHAN FERNANDO, HERATH MUDIYANSELAGE UDARI LAKMINI HERATH and JIN WON HYUN

Department of Biochemistry, College of Medicine and Jeju Research Center for Natural Medicine, Jeju National University, Jeju 63243, Republic of Korea

Received November 21, 2023; Accepted April 11, 2024

DOI: 10.3892/etm.2024.12563

Abstract. Particulate matter 2.5 ($PM_{2.5}$) imposes a heavy burden on the skin and respiratory system of human beings, causing side effects such as aging, inflammation and cancer. Astaxanthin (ATX) is a well-known antioxidant widely used for its anti-inflammatory and anti-aging properties. However, few studies have investigated the protective effects of ATX against $PM_{2.5}$-induced senescence in HaCaT cells. In the present study, the levels of reactive oxygen species (ROS) and antioxidant enzymes were measured after treatment with $PM_{2.5}$. The results revealed that $PM_{2.5}$ generated excessive ROS and reduced the translocation of nuclear factor erythroid 2-related factor 2 (NRF2), subsequently reducing the expression of antioxidant enzymes. However, pretreatment with ATX reversed the ROS levels as well as the expression of antioxidant enzymes. In addition, ATX protected cells from $PM_{2.5}$-induced DNA damage and rescued $PM_{2.5}$-induced cell cycle arrest. The levels of senescence-associated phenotype markers, such as interleukin-1β, matrix metalloproteinases, and β-galactosidase, were increased by exposure to $PM_{2.5}$, however these effects were reversed by ATX. After interfering with NRF2 mRNA expression and exposing cells to $PM_{2.5}$, the levels of ROS and β-galactosidase were higher compared with siControl RNA cells exposed to $PM_{2.5}$. However, ATX inhibited ROS and β-galactosidase levels in both the siControl RNA and the siNRF2 RNA groups. Thus, ATX protects HaCaT keratinocytes from $PM_{2.5}$-induced senescence by partially inhibiting excessive ROS generation via the NRF2 signaling pathway.

Correspondence to: Professor Jin Won Hyun, Department of Biochemistry, College of Medicine and Jeju Research Center for Natural Medicine, Jeju National University, 102 Jejudaehakro, Jeju 63243, Republic of Korea
E-mail: jinwonh@jejunu.ac.kr

*Contributed equally

Key words: particulate matter 2.5, astaxanthin, reactive oxygen species, nuclear factor erythroid 2-related factor 2, senescence

Introduction

An epidemiological study suggested that residential emissions, presumed to contain carbonaceous particles as the most toxic ingredients, globally influence premature mortality (1). In cities, diesel exhaust is a source of particulate matter (PM) from traffic, which constitutes a large proportion of urban dust. Various respiratory conditions, ischemic heart disease and cancer are potentially associated with long-term exposure to PM from traffic (2). $PM_{2.5}$ with an aerodynamic diameter of ≤2.5 μm generates reactive oxygen species (ROS), increases the secretion of proinflammatory cytokines, and induces matrix metalloproteinases (MMPs), leading to senescence in both keratinocytes and dermal fibroblasts (3-6).

The transcription factor nuclear factor erythroid 2-related factor 2 (NRF2) plays an important role in maintaining redox balance by preventing the oxidation of macromolecules such as DNA, lipids and proteins. It does this by increasing the levels of cellular antioxidant enzymes, including superoxide dismutase (SOD), catalase (CAT), glutathione peroxidase (GPX) and heme oxygenase 1 (HO-1) (7). NRF2 can serve as a protective target, inhibiting $PM_{2.5}$-induced redox imbalance and inflammation. Recent studies have shown that natural compounds activate NRF2 signaling to protect cells from $PM_{2.5}$-induced damage (8,9).

Astaxanthin (ATX), a naturally occurring carotenoid dye that can be extracted from algae, yeast, shrimp and other organisms, exhibits significant antioxidant activity (10). Therefore, ATX is considered a potential biological compound for treating inflammation, aging and cardiovascular diseases (11). ATX stimulates the NRF2 signaling pathway to enhance cellular antioxidant and anti-inflammatory capabilities, which have neuroprotective, anti-tumorigenic, antidiabetic and hepatoprotective effects (12). Additionally, ATX depletes ROS, thereby preventing skin photoaging (13). However, only a limited number of studies have investigated the effects of ATX on $PM_{2.5}$-induced skin senescence. In the present study, the response of the antioxidant system and senescence were

examined in HaCaT cells exposed to $PM_{2.5}$, as well as the anti-senescence mechanism of ATX.

Materials and methods

Preparation of ATX and $PM_{2.5}$. ATX (cat. no. SML0982; Sigma-Aldrich; Merck KGaA) was dissolved in dimethyl sulfoxide (DMSO). $PM_{2.5}$ (NIST PM; cat. no. SRM 1650b; Sigma-Aldrich; Merck KGaA) was dispersed in DMSO to prepare a stock solution (25 mg/ml). The 50 μg/ml of $PM_{2.5}$ was selected as the optimal concentration based on our previous research (4).

Cell culture. HaCaT (cat. no. 300493; CLS Cell Lines Service GmbH) cells were seeded in Dulbecco's modified Eagle's medium (Thermo Fisher Scientific, Inc.) supplemented with 10% heat-inactivated fetal calf serum (Thermo Fisher Scientific, Inc.) and 1% antibiotic-antimycotic solution in 5% CO_2 at 37˚C.

Cell viability. Cells were cultured in a 24-well plate with ATX (1, 2.5, 5, 7.5 and 10 μM) and/or $PM_{2.5}$ for 48 h at 37˚C. Subsequently, 100 μl 3-(4,5-dimethylthiazol-2-yl)-2,5-diphenyltetrazolium bromide (cat. no. 475989; Sigma-Aldrich; Merck KGaA) was added to each well to form an insoluble purple formazan by the action of mitochondrial reductase in live cells at 37˚C for 4 h, which was dissolved in 600 μl DMSO. The solution was then transferred to a 96-well plate and observed using a scanning multi-well spectrophotometer at 540 nm.

ROS detection. 2',7'-Dichlorodihydrofluorescein diacetate (H_2DCFDA) (cat. no. D6883; Sigma-Aldrich; Merck KGaA), a cell-permeant ROS probe, was used to measure intracellular ROS content in HaCaT cells. Cells were cultured with ATX (1, 2.5, 5 and 7.5 μM) or a ROS scavenger (1 mM N-acetyl cysteine, NAC) (cat. no. A9165; Sigma-Aldrich; Merck KGaA) and then exposed to 1 mM H_2O_2 or 50 μg/ml $PM_{2.5}$. After staining with H_2DCFDA, fluorescence in the cells was detected individually using fluorescence spectrometer (Promega Corporation) and BD LSR II flow cytometer with FACSDIVA software version 6.0 (Becton, Dickinson and Company). Similarly, siControl and siNRF2 cells were cultured with ATX or NAC and exposed to $PM_{2.5}$. ROS levels were measured using a confocal microscope (Olympus Corporation).

Western blot analysis. Cell lysis was performed using the PRO-PREP™ protein extraction solution (cat. no. 17081; Intron Biotechnology, Inc.) or the NE-PER™ nuclear and cytoplasmic extraction reagents (cat. no. 78833; Thermo Fisher Scientific, Inc.). The protein concentration was determined using a BCA assay kit (cat. no. 23225; Thermo Fisher Scientific, Inc.). Subsequently, 40 μg cell lysates were separated by electrophoresis on a 10 or 12% SDS-polyacrylamide gel and were transferred onto PVDF membranes. The membranes were subjected to blocking in 3% bovine serum albumin (Bovogen Biologicals Pty Ltd.) for 1 h at 20˚C with agitation, incubation with primary antibodies (1:1,000) for 2 h at 20˚C, and incubation with HRP-conjugated secondary antibodies (1:5,000; anti-rabbit, cat. no. ab6721 and anti-mouse, cat. no. ab205719; Abcam) for 2 h at 20˚C. The membranes were then washed with 1X TBS-0.1% Tween-20 (cat. no. 9997; Cell Signaling Technology, Inc.). Subsequently, the membranes with the targeted proteins were exposed to an enhanced chemiluminescence reagent (Cytiva) and the corresponding bands were visualized using an autoradiography film. The following primary antibodies were used: NRF2 (cat. no. sc-722), CAT (cat. no. sc-271803), GPX1/2 (cat. no. sc-133160), cyclin dependent kinase inhibitor 2A (p16) (cat. no. sc-1661), HO-1 (cat. no. sc-390991) and actin (cat. no. sc-8432) were purchased from Santa Cruz Biotechnology, Inc. Phospho-H2A histone family member X (H2A.X; cat. no. 2577), H2A.X (cat. no. 2595), c-Fos (cat. no. 2250), jun proto-oncogene, activator protein-1 (AP-1) transcription factor subunit (c-Jun; cat. no. 9165), phospho-c-Jun (cat. no. 91952) were obtained from Cell Signaling Technology, Inc. Phospho-NRF2 (cat. no. ab76026), interleukin (IL)-1β (cat. no. ab315084), MMP-2 (cat. no. ab92536), MMP-9 (cat. no. ab76003) and TATA-binding protein (TBP) (cat. no. ab818) were purchased from Abcam. Cu/Zn SOD (cat. no. ADI-SOD-100) was purchased from Enzo Life Sciences, Inc. Protein bands were analyzed using ImageJ version 1.48V (National Institutes of Health).

Detection of 8-oxoguanine DNA glycosylase (8-oxoG). The avidin-tetra-methyl-rhodamine isothiocyanate (TRITC) conjugate (cat. no. A7169; Sigma-Aldrich; Merck KGaA) exhibited highly specific binding to oxidized nucleosides 8-oxoG (14). The cells were stained with avidin-TRITC dye for 30 min at 37˚C and observed under a confocal microscope.

Cell cycle analysis. Cells were cultured with ATX or/and $PM_{2.5}$ treatment in 6-well plates at 37˚C for 24 h, after which, they were fixed with 70% ethanol for 1 h at 4˚C, and stained with propidium iodide (cat. no. P4864; Sigma-Aldrich; Merck KGaA) and RNase A (1:1,000; cat. no. 12091-021; Thermo Fisher Scientific, Inc.) at 37˚C for 1 h. Cellular DNA content was detected using FACSCalibur flow cytometer with CellQuest pro software 4.02 (Becton, Dickinson and Company) for cell cycle analysis.

β-Galactosidase staining assay. Senescence-associated β-galactosidase (SA-β-Gal) expressed in senescent cells was detected using a cellular senescence detection kit (SPiDER-β-Gal) (cat. no. SG03; Dojindo Laboratories, Inc.). Images and histograms were obtained using flow cytometry and confocal microscopy, respectively.

Transient transfection of small interfering RNA (siRNA). Lipofectamine® RNAiMax (cat. no. 13778075; Thermo Fisher Scientific, Inc.) was used to transfect 20 nM siRNA against NRF2 (siNRF2 RNA) (cat. no. sc-37030; Santa Cruz Biotechnology, Inc.) or negative control (siControl RNA) (cat. no. sc-37007; Santa Cruz Biotechnology, Inc.) into cells. The siRNA sequences were as follows: Control siRNA sense, 5'-CACAGGGUAAGGAACUCGUCUCUCA-3' and antisense, 5'-UGAGAGACGAGUUCCUUACCCUGUG-3'; and NRF2 siRNA sense, 5'-GCAUGCUACGUGAUGAAG Att-3' and antisense, 5'-UCUUCAUCACGUAGCAUGCtt-3'. After incubation for 24 h at 37˚C, the transfected cells were

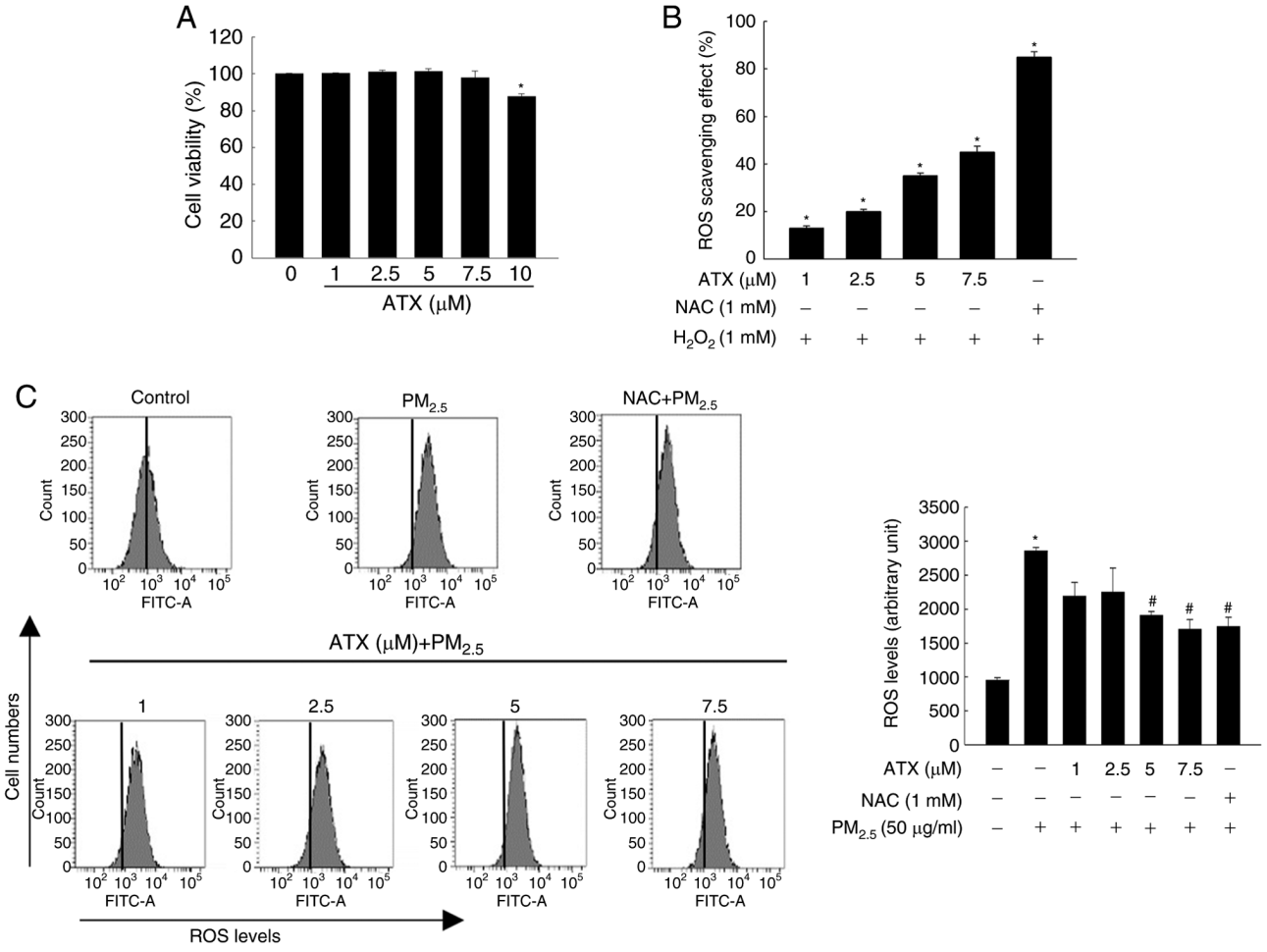

Figure 1. Inhibitory effect of ATX on H_2O_2- or $PM_{2.5}$-induced intracellular ROS. (A) Viability of HaCaT cells cultured with 1, 2.5, 5, 7.5 and 10 μM ATX was detected using the MTT assay. *P<0.05 vs. ATX-untreated cells. (B and C) Cells were cultured with 1, 2.5, 5 and 7.5 μM ATX, 1 mM NAC, 1 mM H_2O_2, or 50 μg/ml $PM_{2.5}$. ROS scavenging effects were measured (B) via fluorescence spectrometer (*P<0.05 vs. H_2O_2-treated cells) and (C) through flow cytometry after staining with H_2DCFDA (*P<0.05 vs. the $PM_{2.5}$-untreated cells; #P<0.05 vs. $PM_{2.5}$-treated cells). ATX, astaxanthin; $PM_{2.5}$, particulate matter 2.5; ROS, reactive oxygen species; NAC, N-acetyl cysteine.

processed for ROS detection and β-galactosidase staining assay.

Statistical analysis. All the values of measurements are expressed as the mean ± standard deviation. The results were analyzed for pairwise differences using one-way analysis of variance followed by Tukey's post hoc test. P<0.05 was considered to indicate a statistically significant difference. Statistical analysis was performed using SigmaStat v3.5 (Systat Software Inc.).

Results

ATX scavenges ROS generated from $PM_{2.5}$. HaCaT cells were cultured with ATX (0, 1, 2.5, 5, 7.5 and 10 μM) for 48 h at 37˚C. Cell viability assay results revealed that ATX had no cytotoxicity at a concentration <7.5 μM (Fig. 1A). The ROS scavenging effects of ATX were then examined. Cells were pretreated with ATX (1, 2.5, 5 and 7.5 μM) or NAC (1 mM). The production of H_2O_2-induced intracellular ROS was inhibited significantly by ATX or NAC (Fig. 1B). In addition, ATX inhibited ROS generation from $PM_{2.5}$ (Fig. 1C). According to the results, 7.5 μM ATX was selected as the optimal concentration in further experiments.

ATX recovers the homeostasis of the antioxidant enzymes by activating NRF2. To maintain cellular homeostasis, NRF2 plays an important role in the regulation of oxidative stress by activating antioxidant enzymes (SOD, CAT, GPX and HO-1) to eliminate ROS (7). In the present study, the active form of NRF2 in nuclear fraction and the expression levels of antioxidant enzymes were tested. After $PM_{2.5}$ treatment, the expression of phospho-NRF2 was the highest in the first 12 h and then decreased gradually (Fig. 2A). Conversely, it increased gradually in a time-dependent manner up to 72 h after ATX pretreatment (Fig. 2B). Accordingly, phospho-NRF2 levels in the nuclear fraction, which were reduced after $PM_{2.5}$ exposure for 48 h, increased after pretreatment with ATX (Fig. 2C). The expression of Cu/Zn SOD, CAT and GPX1/2 decreased following treatment with $PM_{2.5}$ in a dose-dependent manner; HO-1 expression was elevated at 12 and 24 h and then decreased significantly after exposure to $PM_{2.5}$ (Fig. 2D). However, the reduced levels of Cu/Zn SOD, CAT, GPX1/2, and HO-1 following

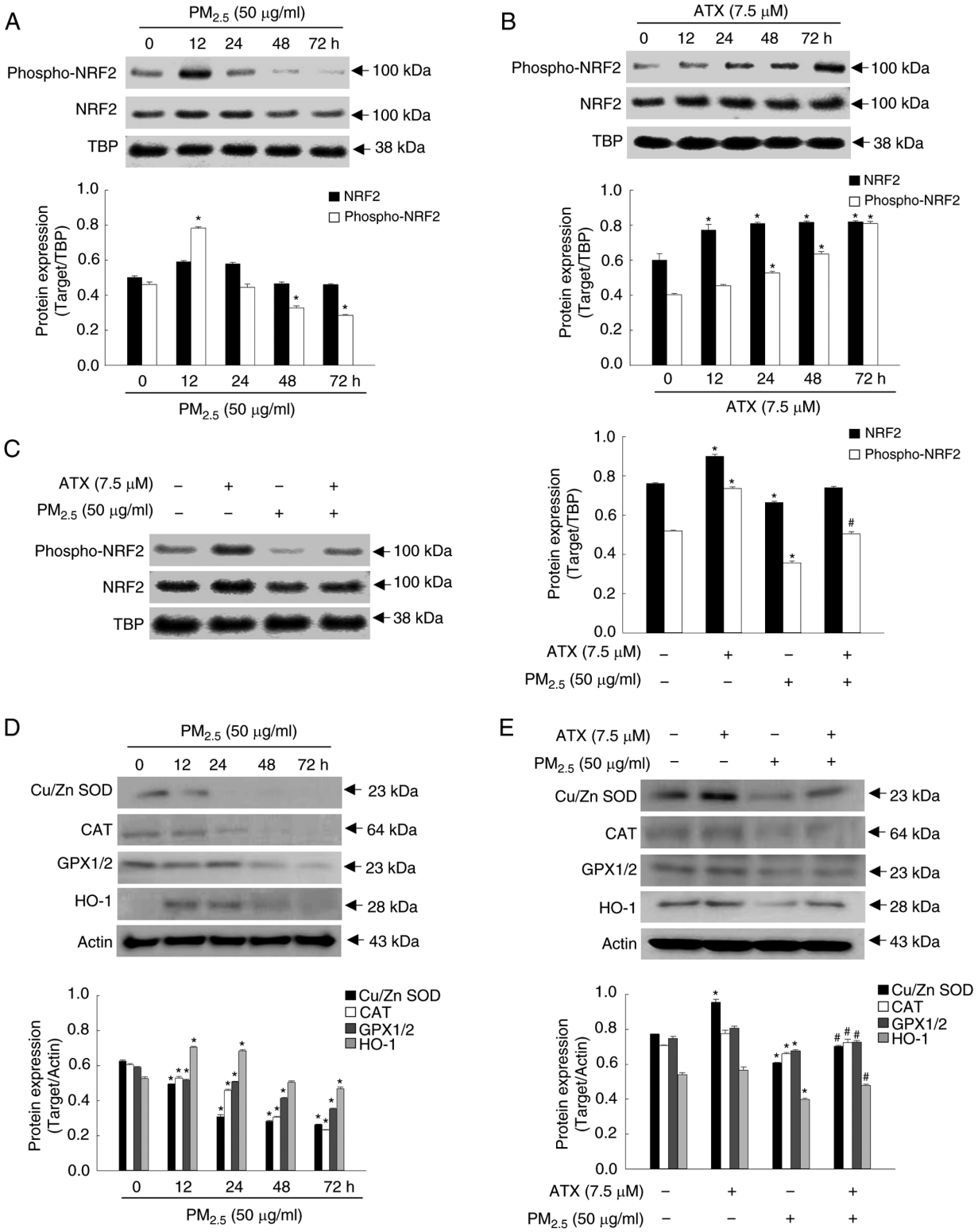

Figure 2. Recovery effect of ATX on antioxidant-related mediator inhibited by $PM_{2.5}$. (A and B) The protein levels of phospho-NRF2 and NRF2, after (A) $PM_{2.5}$ or (B) ATX treatment for various time intervals were detected by western blotting. TBP was used a nuclear fraction loading control. *P<0.05 vs. $PM_{2.5}$ or ATX-untreated cells at 0 h. (C) The protein levels of phospho-NRF2 and NRF2 after treatment with ATX and/or $PM_{2.5}$ were detected by western blotting. *P<0.05 vs. ATX or $PM_{2.5}$-untreated cells; $^{\#}$P<0.05 vs. $PM_{2.5}$-treated cells. (D) The protein levels of Cu/Zn SOD, CAT, GPX1/2 and HO-1 after $PM_{2.5}$ treatment at various time intervals were detected by western blotting. Actin was used as a loading control. *P<0.05 vs. $PM_{2.5}$-untreated cells at 0 h. (E) The protein levels of Cu/Zn SOD, CAT, GPX1/2 and HO-1 after cells were treated with ATX and/or $PM_{2.5}$ were detected by western blot analysis. *P<0.05 vs. ATX or $PM_{2.5}$-untreated cells; $^{\#}$P<0.05 vs. $PM_{2.5}$-treated cells. ATX, astaxanthin; $PM_{2.5}$, particulate matter 2.5; TBP, TATA-binding protein; NRF2, nuclear factor erythroid 2-related factor 2; SOD, superoxide dismutase; CAT, catalase; GPX1/2, glutathione peroxidase 1/2; HO-1, heme oxygenase 1.

$PM_{2.5}$ exposure were increased after pretreatment with ATX (Fig. 2E). Therefore, it was revealed that ATX restored intracellular redox homeostasis by activating NRF2 and its related enzymes, which were decreased by $PM_{2.5}$.

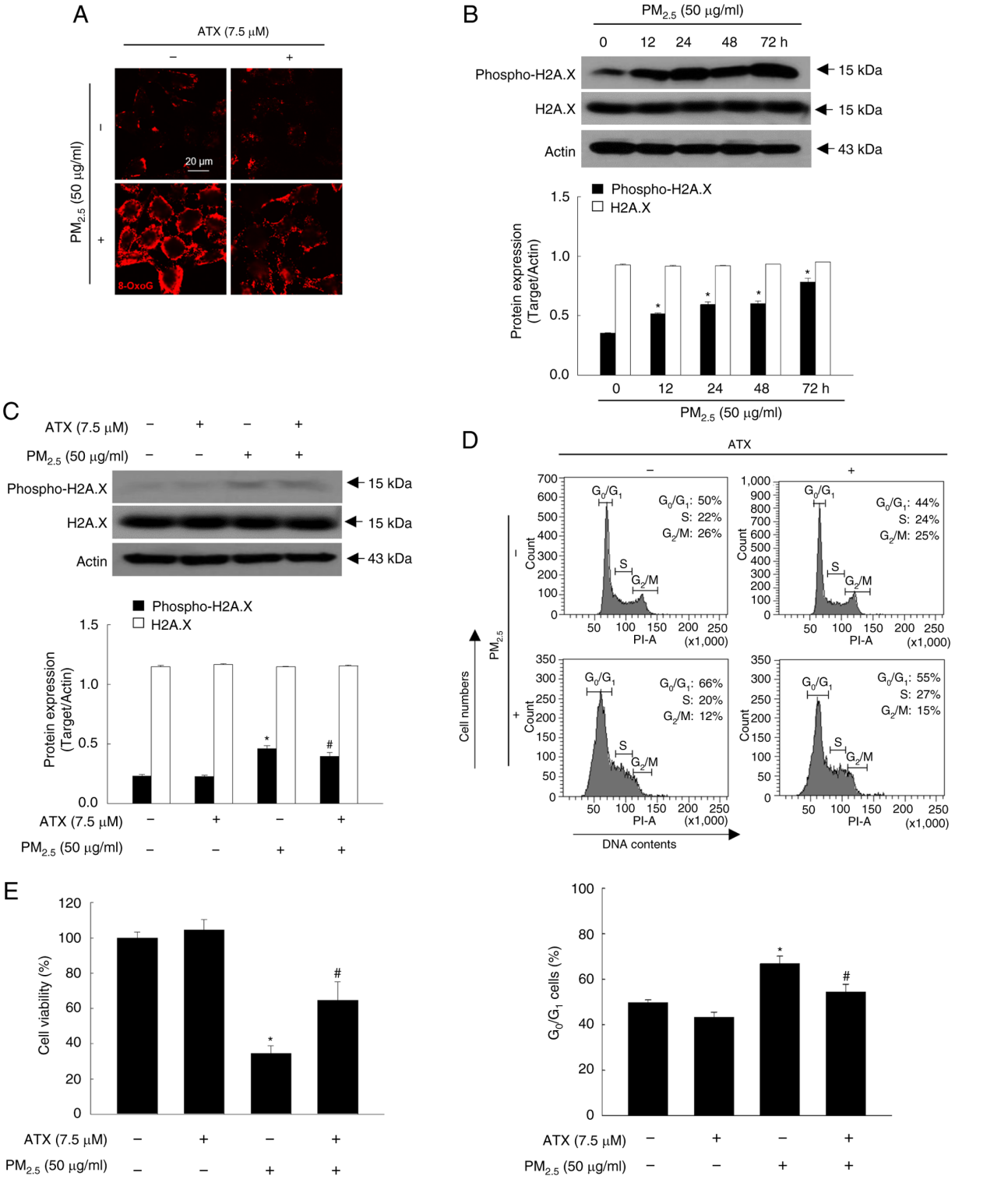

Figure 3. Protective effect of ATX on $PM_{2.5}$-induced DNA damage and cell cycle arrest. (A) The intracellular levels of 8-oxoG were measured by confocal microscopy after staining of avidin-TRITC. (B) Phospho-H2A.X and total H2A.X levels after $PM_{2.5}$ treatment at various time intervals were detected by western blotting. *P<0.05 vs. $PM_{2.5}$-untreated cells at 0 h. (C) Phospho-H2A.X and total H2A.X levels after treatment with ATX and/or $PM_{2.5}$ were detected by western blotting. *P<0.05 vs. ATX or $PM_{2.5}$-untreated cells; #P<0.05 vs. $PM_{2.5}$-treated cells. (D) Cell cycle was detected by flow cytometry after staining with propidium iodide. *P<0.05 vs. ATX or $PM_{2.5}$-untreated cells; #P<0.05 vs. $PM_{2.5}$-treated cells. (E) Cell viability was measured by MTT assay. *P<0.05 vs. ATX or $PM_{2.5}$-untreated cells; #P<0.05 vs. $PM_{2.5}$-treated cells. ATX, astaxanthin; $PM_{2.5}$, particulate matter 2.5; 8-oxoG, 8-oxoguanine DNA glycosylase; H2A.X, H2A histone family member X.

ATX protects cells from $PM_{2.5}$-induced DNA damage. 8-OxoG and phospho-H2A.X are two specific markers of DNA damage and present in high levels in the $PM_{2.5}$ treatment group of keratinocytes (14). According to the results, ATX showed protective effects from $PM_{2.5}$-induced nucleoside oxidization and phospho-H2A.X expression (Fig. 3A-C). Cell cycle checkpoints monitor DNA damage and the response to cell cycle by DNA damage is executed by a cell cycle control

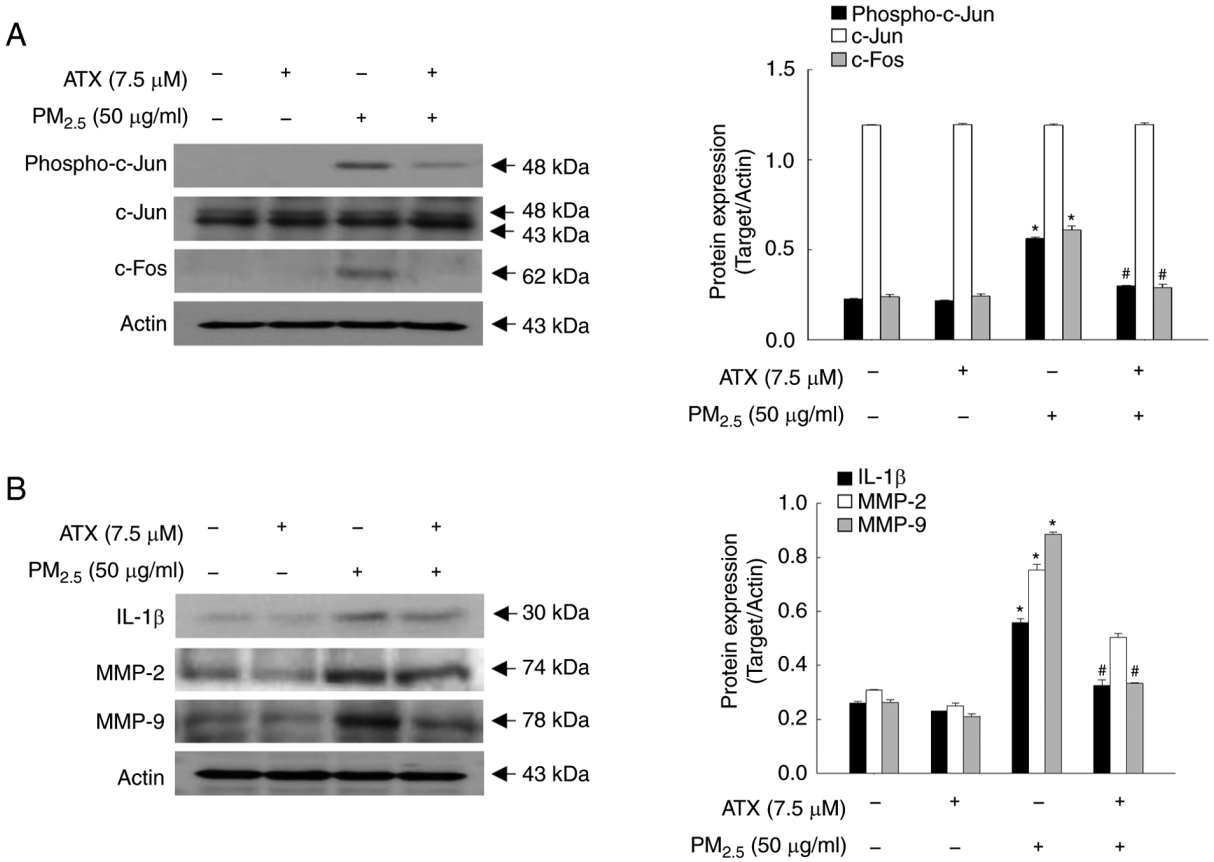

Figure 4. Inhibitory effects of ATX on $PM_{2.5}$-induced transcription factor, AP-1, pro-inflammatory cytokines and MMPs. (A and B) Western blot assay was performed for the detection of (A) protein levels of phospho-c-Jun, c-Jun, c-Fos, and (B) protein levels of IL-1β, MMP-2 and MMP-9. *P<0.05 vs. ATX or $PM_{2.5}$-untreated cells; $^{\#}$P<0.05 vs. $PM_{2.5}$-treated cells. MMPs, matrix metalloproteinases; c-Jun, jun proto-oncogene, AP-1 transcription factor subunit; c-Fos, fos proto-oncogene, AP-1 transcription factor subunit.

mechanism (15). $PM_{2.5}$ perturbed the cell cycle, causing G_0/G_1 arrest, which was reversed by ATX treatment (Fig. 3D). ATX also improved cell viability, which had been reduced by exposure to $PM_{2.5}$ (Fig. 3E). Therefore, ATX exhibited DNA protective effects, inhibited cell cycle arrest, and promoted cell viability in $PM_{2.5}$-treated cells.

ATX inhibits the secretion of $PM_{2.5}$-induced cytokine and MMPs. Cellular senescence is caused by damaging stimuli that contribute to an irreversible state of cell cycle arrest, in which cytokines and MMPs are secreted (16). In addition, AP-1, which comprises the transcription factors c-Fos and c-Jun, is highly regulated by UV light during photoaging and closely related to the expression of ILs and MMPs (17). In the present study, the protein levels of phospho-c-Jun and c-Fos were increased significantly by $PM_{2.5}$, whereas they were decreased by pretreatment with ATX (Fig. 4A). Cytokines, such as IL-1β, MMP-2 and MMP-9, were expressed at higher levels in $PM_{2.5}$-treated group than in the control group; however, they were inhibited by treatment with ATX (Fig. 4B). Therefore, ATX protected keratinocytes from $PM_{2.5}$-induced senescence-associated cytokines and MMPs.

ATX protects cells from $PM_{2.5}$-induced senescence-associated secretory phenotype (SASP). p16 and SA-β-Gal are the key markers of SASP, which indicates the state of skin aging (18). Therefore, in the present study, p16 protein expression in keratinocytes was examined over time among the four groups. The p16 level increased up to 48 h by $PM_{2.5}$ (Fig. 5A) and was decreased upon pretreatment with ATX (Fig. 5B). Moreover, ATX inhibited cellular SA-β-Gal, which was observed by flow cytometry (Fig. 5C) and confocal microscopy (Fig. 5D). Therefore, ATX protected keratinocytes from $PM_{2.5}$-induced senescence.

ATX attenuates $PM_{2.5}$-induced senescence by inhibiting ROS via the NRF2. To confirm the role of NRF2 in $PM_{2.5}$-induced senescence, a siRNA was used to interfere with NRF2 mRNA expression. After exposure to $PM_{2.5}$, the ROS levels were significantly higher in cells transfected with siNRF2 RNA than in those transfected with siControl RNA, which was inhibited by treatment with ATX and NAC (Fig. 6A). After exposure to $PM_{2.5}$, cells transfected with siNRF2 RNA showed higher SA-β-Gal fluorescence than siControl RNA cells, a phenomenon that was decreased significantly by ATX treatment (Fig. 6B). Therefore, ROS amelioration of ATX relieved senescence induced by $PM_{2.5}$ through the NRF2 pathway.

Discussion

$PM_{2.5}$ is currently a major concern, and research is underway to understand its effects on the human body. The human

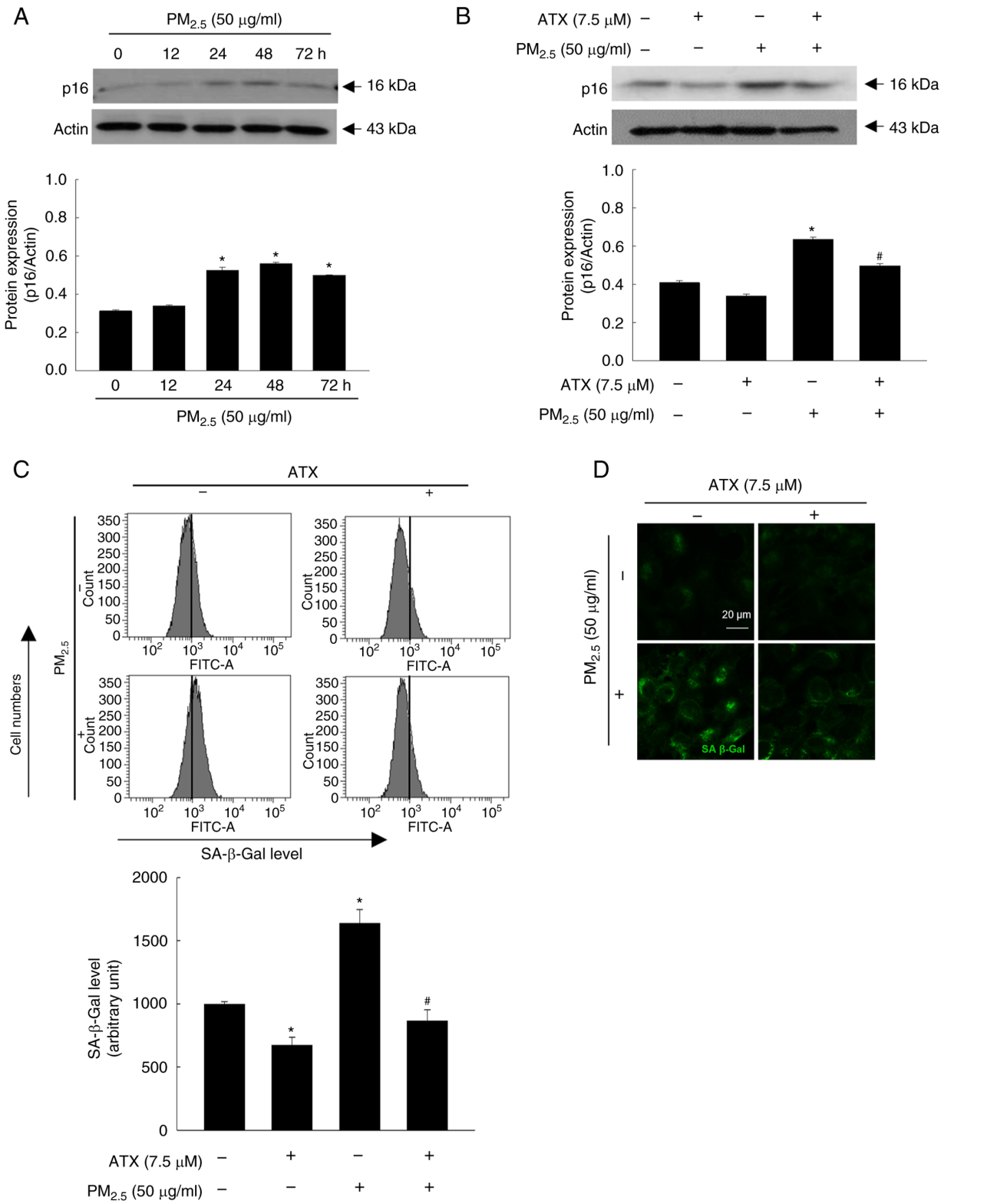

Figure 5. Inhibitory effect of ATX on $PM_{2.5}$-induced senescence. (A) p16 levels after $PM_{2.5}$ treatment at various time intervals were detected by western blot analysis. (B) p16 levels after cells were treated with ATX and/or $PM_{2.5}$ were detected by western blotting. (C and D) Cells were stained using SPiDER-β-Gal and the senescent cells were detected by (C) flow cytometry and (D) confocal microscopy. Green fluorescence was observed in the cytoplasm of senescent cells, indicating elevated SA-β-gal activity. *P<0.05 vs. ATX or $PM_{2.5}$-untreated cells; #P<0.05 vs. $PM_{2.5}$-treated cells. ATX, astaxanthin; $PM_{2.5}$, particulate matter 2.5; p16, cyclin dependent kinase inhibitor 2A; SA-β-gal, senescence-associated beta-galactosidase,

skin acts as the first barrier against environmental stress, however $PM_{2.5}$ can penetrate this barrier and cause skin problems. Previous studies by the authors have demonstrated that $PM_{2.5}$ could penetrate skin cells and damage the skin by inducing oxidative stress (3-5). This leads to the destruction of cellular macromolecules and organelles, as well as apoptotic cell death (4). It was also revealed that $PM_{2.5}$ activates the inflammatory pathway toll-like receptor 5-NADPH oxidase

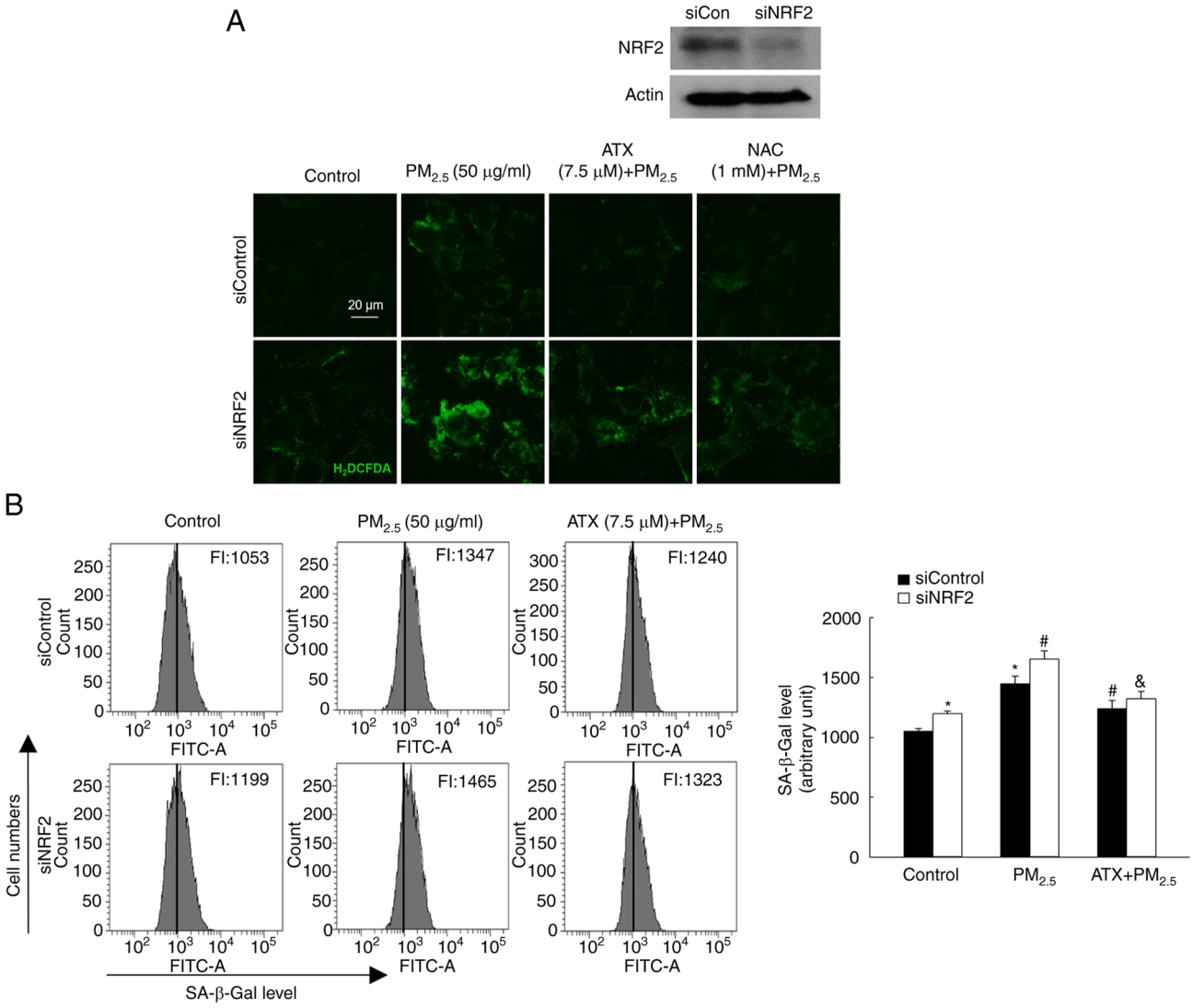

Figure 6. Inhibitory effect of ATX on $PM_{2.5}$-induced senescence via the NRF2. (A and B) After transfection of cells with siRNA against NRF2, (A) ROS levels of the siControl RNA and siNRF2 RNA groups were measured using a confocal microscope by H_2DCFDA staining, with green fluorescence indicating elevated intracellular ROS levels, and (B) SA-β-gal activity was detected using flow cytometry. *P<0.05 vs. siControl RNA group; $^{\#}$P<0.05 vs. $PM_{2.5}$-treated siControl RNA group; $^{\&}$P<0.05 vs. ATX and $PM_{2.5}$-treated siControl RNA group. ATX, astaxanthin; $PM_{2.5}$, particulate matter 2.5; NRF2, nuclear factor erythroid 2-related factor 2; si-, small interfering; ROS, reactive oxygen species; SA-β-gal, senescence-associated beta-galactosidase.

4-NFκB-IL-6 in both wild-type mice and flaky tail mice. This suggested that $PM_{2.5}$-induced inflammation may contribute to the development and exacerbation of atopic dermatitis (3). Furthermore, it was revealed that $PM_{2.5}$ induced skin senescence by the aryl hydrocarbon receptor-ROS-p16 pathway via epigenetic modification (19). These findings suggested that ROS are key factors in the induction of inflammation and aging by $PM_{2.5}$, and a solution in natural products was sought. Previously, various studies have revealed that various natural compounds from marine algae can decrease excessive ROS levels in skin cells (20,21). In addition, agar oligosaccharide, a marine prebiotic, has anti-aging effects via the activation of antioxidant enzymes, such as Cu/Zn SOD and CAT, in *Drosophila melanogaster* (22). Moreover, oligosaccharides from green algae have anti-aging effects by increasing CAT and GSH levels and decreasing lipid oxidation levels in mice (23).

ATX, a potent antioxidant, has been demonstrated to mitigate the physiological adverse effects of oxidative stress during the senescence process and extend lifespan both *in vitro* and *in vivo* (24). Furthermore, ATX has been revealed to alleviate oxidative stress and immune impairment in rats with galactose-induced aging by activating the NRF2/KEAP1 pathway and suppressing the NFκB pathway (25). In the present study, it was aimed to investigate the beneficial effects of ATX isolated from algae, on $PM_{2.5}$-induced DNA damage, cell cycle arrest and senescence in HaCaT cells. As demonstrated in Fig. 1C, ATX pretreatment inhibited $PM_{2.5}$-induced cellular ROS generation. The data of the present study also revealed that ATX increased the activation of NRF2 and the expression of antioxidant-related proteins that are downregulated by $PM_{2.5}$ (Fig. 2). These results indicated that ATX suppressed $PM_{2.5}$-induced ROS generation through the activation of the NRF2-antioxidant enzyme pathways.

$PM_{2.5}$-induced oxidative stress causes DNA damage, which leads to cell cycle arrest in skin cells (26). The data of the present study revealed that ATX decreased base modification or breakage of DNA damage in $PM_{2.5}$-treated cells

(Fig. 3A-C). Oxidative stress-induced DNA damage is one way to induce senescence and can maintain G_1 confinement, accelerating aging under stress (27). The results of the present study demonstrated that $PM_{2.5}$ stimulated G_1 arrest. However, treatment with ATX reversed the effects (Fig. 3D). A previous study revealed that $PM_{2.5}$ induces MMPs via the AP-1 signaling pathway through ROS generation (26). In addition, ROS increase the secretion of pro-inflammatory cytokines to high levels in most senescent cells (28). In the present study, it was demonstrated that $PM_{2.5}$ activated the transcription factor of inflammatory cytokines, AP-1 (Fig. 4A), followed by the secretion of pro-inflammatory cytokines and MMPs (Fig. 4B). However, ATX inhibited the AP-1, cytokine and MMP secretion induced by $PM_{2.5}$. DNA damage has been considered an activator of SASP associated with cell cycle arrest (15). IL-1β and IL-6 are the most important SASP factors and have been detected at high levels in senescent cells (28). Furthermore, the expression of a senescence marker, p16, and β-galactosidase activity were stimulated by $PM_{2.5}$; however, these decreased upon pretreatment with ATX (Fig. 5).

Several studies have reported that NRF2, a regulator of antioxidant enzymes, plays a role in anti-aging mechanisms (29-31). The active form of vitamin D, $1,25(OH)_2D_3$, also plays a role in delaying aging. It does this by upregulating NRF2, inhibiting oxidative stress and DNA damage, inactivating the p53-p21 and p16-Rb signaling pathways, and inhibiting cellular senescence and SASP (29). Furthermore, ATX is reported to have anti-inflammatory properties and exerts its protective effects by stimulating the NRF2 signaling pathway (14). The results of the present study revealed that NRF2 knockdown increased the β-galactosidase activity induced by $PM_{2.5}$; however ATX decreased the β-galactosidase activity (Fig. 6), suggesting that ATX inhibited $PM_{2.5}$-induced senescent cells through NRF2.

In conclusion, the induction of the antioxidant system through NRF2 upregulation by ATX resulted in inhibiting the generation of ROS by $PM_{2.5}$ and the DNA damage response, thereby preventing cell cycle arrest. Additionally, ATX inhibited the AP-1 signaling pathway, thereby reversing the secretion of pro-inflammatory cytokines and MMPs, ultimately inhibiting $PM_{2.5}$-induced senescence. Notably, ATX exhibited an anti-$PM_{2.5}$-induced senescence effect and could be utilized as a preventive agent against air pollution-triggered skin aging.

Acknowledgements

Not applicable.

Funding

The present study was supported by (grant no. RS-2023-00270936) the Basic Science Research Program through the National Research Foundation of Korea (NRF), funded by the Ministry of Education.

Availability of data and materials

The data generated in the present study may be requested from the corresponding author.

Authors' contributions

KAK, AXZ and JWH conceived and designed the present study, and wrote the main manuscript. KAK, AXZ and MJP performed the experiments and acquired data. PDSMF and HMULH analyzed and interpreted the data, and performed the literature searches. KAK and JWH confirm the authenticity of the raw data. All authors have read and approved the final manuscript.

Ethics approval and consent to participate

Not applicable.

Patient consent for publication

Not applicable.

Competing interests

The authors declare that they have no competing interests.

References

1. Lelieveld J, Evans JS, Fnais M, Giannadaki D and Pozzer A: The contribution of outdoor air pollution sources to premature mortality on a global scale. Nature 525: 367-371, 2015.
2. Boogaard H, Patton AP, Atkinson RW, Brook JR, Chang HH, Crouse DL, Fussell JC, Hoek G, Hoffmann B, Kappeler R, *et al*: Long-term exposure to traffic-related air pollution and selected health outcomes: A systematic review and meta-analysis. Environ Int 164: 107262, 2022.
3. Ryu YS, Kang KA, Piao MJ, Ahn MJ, Yi JM, Hyun YM, Kim SH, Ko MK, Park CO and Hyun JW: Particulate matter induces inflammatory cytokine production via activation of NFκB by TLR5-NOX4-ROS signaling in human skin keratinocyte and mouse skin. Redox Biol 21: 101080, 2019.
4. Piao MJ, Ahn MJ, Kang KA, Ryu YS, Hyun YJ, Shilnikova K, Zhen AX, Jeong JW, Choi YH, Kang HK, *et al*: Particulate matter 2.5 damages skin cells by inducing oxidative stress, subcellular organelle dysfunction, and apoptosis. Arch Toxicol 92: 2077-2091, 2018.
5. Hyun YJ, Piao MJ, Kang KA, Zhen AX, Madushan Fernando PDS, Kang HK, Ahn YS and Hyun JW: Effect of fermented fish oil on fine particulate matter-induced skin aging. Mar Drugs 17: 61, 2019.
6. Reynolds WJ, Hanson PS, Critchley A, Griffiths B, Chavan B and Birch-Machin MA: Exposing human primary dermal fibroblasts to particulate matter induces changes associated with skin aging. FASEB J 34: 14725-14735, 2020.
7. Mendonça ELSS, Xavier JA, Fragoso MBT, Silva MO, Escodro PB, Oliveira ACM, Tucci P, Saso L and Goulart MOF: E-stilbenes, general chemical and biological aspects, potential pharmacological activity based on the Nrf2 pathway. Pharmaceuticals (Basel) 17: 232, 2024.
8. Zhang LM, Lv SS, Fu SR, Wang JQ, Liang LY, Li RQ, Zhang F and Ma YX: Procyanidins inhibit fine particulate matter-induced vascular smooth muscle cells apoptosis via the activation of the Nrf2 signaling pathway. Ecotoxicol Environ Saf 223: 112586, 2021.
9. Kahremany S, Hofmann L, Eretz-Kdosha N, Silberstein E, Gruzman A and Cohen G: SH-29 and SK-119 attenuates air-pollution induced damage by activating Nrf2 in HaCaT cells. Int J Environ Res Public Health 18: 12371, 2021.
10. Han SI, Chang SH, Lee C, Jeon MS, Heo YM, Kim S and Choi YE: Astaxanthin biosynthesis promotion with pH shock in the green microalga, Haematococcus lacustris. Bioresour Technol 314: 123725, 2020.
11. Kumar S, Kumar R, Diksh, Kumari A and Panwar A: Astaxanthin: A super antioxidant from microalgae and its therapeutic potential. J Basic Microbiol 62: 1064-1082, 2022.

12. Ashrafizadeh M, Ahmadi Z, Yaribeygi H, Sathyapalan T and Sahebkar A: Astaxanthin and Nrf2 signaling pathway: A novel target for new therapeutic approaches. Mini Rev Med Chem 22: 312-321, 2022.
13. Imokawa G: Intracellular signaling mechanisms involved in the biological effects of the xanthophyll carotenoid astaxanthin to prevent the photo-aging of the skin in a reactive oxygen species depletion-independent manner: The key role of mitogen and stress-activated protein kinase 1. Photochem Photobiol 95: 480-489, 2019.
14. Zhen AX, Piao MJ, Hyun YJ, Kang KA, Madushan Fernando PDS, Cho SJ, Ahn MJ and Hyun JW: Diphlorethohydroxycarmalol attenuates fine particulate matter-induced subcellular skin dysfunction. Mar Drugs 17: 95, 2019.
15. Matthews HK, Bertoli C and de Bruin RAM: Cell cycle control in cancer. Nat Rev Mol Cell Biol 23: 74-88, 2022.
16. Hernandez-Segura A, Nehme J and Demaria M: Hallmarks of cellular senescence. Trends Cell Biol 28: 436-453, 2018.
17. Oh JH, Joo YH, Karadeniz F, Ko J and Kong CS: Syringaresinol inhibits UVA-induced MMP-1 expression by suppression of MAPK/AP-1 signaling in HaCaT keratinocytes and human dermal fibroblasts. Int J Mol Sci 21: 3981, 2020.
18. Samdavid Thanapaul RJR, Shvedova M, Shin GH, Crouch J and Roh DS: Elevated skin senescence in young mice causes delayed wound healing. Geroscience 44: 1871-1878, 2022.
19. Ryu YS, Kang KA, Piao MJ, Ahn MJ, Yi JM, Bossis G, Hyun YM, Park CO and Hyun JW: Particulate matter-induced senescence of skin keratinocytes involves oxidative stress-dependent epigenetic modifications. Exp Mol Med 51: 1-14, 2019.
20. Zhen AX, Piao MJ, Kang KA, Fernando PD, Herath HM, Cho SJ and Hyun JW: 3-Bromo-4,5-dihydroxybenzaldehyde protects keratinocytes from particulate matter 2.5-induced damages. Antioxidants (Basel) 12: 1307, 2023.
21. Wang L, Lee W, Jayawardena TU, Cha SH and Jeon YJ: Dieckol, an algae-derived phenolic compound, suppresses airborne particulate matter-induced skin aging by inhibiting the expressions of pro-inflammatory cytokines and matrix metalloproteinases through regulating NF-κB, AP-1, and MAPKs signaling pathways. Food Chem Toxicol 146: 111823, 2020.
22. Ma C, Yang K, Wang Y and Dai X: Anti-aging effect of agar oligosaccharide on male Drosophila melanogaster and its preliminary mechanism. Mar Drugs 17: 632, 2019.
23. Liu XY, Liu D, Lin GP, Wu YJ, Gao LY, Ai C, Huang YF, Wang MF, El-Seedi HR, Chen XH and Zhao C: Anti-ageing and antioxidant effects of sulfate oligosaccharides from green algae Ulva lactuca and Enteromorpha prolifera in SAMP8 mice. Int J Biol Macromol 139: 342-351, 2019.
24. Sorrenti V, Davinelli S, Scapagnini G, Willcox BJ, Allsopp RC and Willcox DC: Astaxanthin as a putative geroprotector: Molecular basis and focus on brain aging. Mar Drugs 18: 351, 2020.
25. Chen Z, Xiao J, Liu H, Yao K, Hou X, Cao Y and Liu X: Astaxanthin attenuates oxidative stress and immune impairment in D-galactose-induced aging in rats by activating the Nrf2/Keap1 pathway and suppressing the NF-κB pathway. Food Funct 11: 8099-8111, 2020.
26. Herath HMUL, Piao MJ, Kang KA, Zhen AX, Fernando PDSM, Kang HK, Yi JM and Hyun JW: Hesperidin exhibits protective effects against PM2.5-mediated mitochondrial damage, cell cycle arrest, and cellular senescence in human HaCaT keratinocytes. Molecules 27: 4800, 2022.
27. Kumari R and Jat P: Mechanisms of cellular senescence: Cell cycle arrest and senescence associated secretory phenotype. Front Cell Dev Biol 9: 645593, 2021.
28. Zhou Q, Wang W, Wu J, Qiu S, Yuan S, Fu PL, Qian QR and Xu YZ: Ubiquitin-specific protease 3 attenuates interleukin-1β-mediated chondrocyte senescence by deacetylating forkhead box O-3 via sirtuin-3. Bioengineered 13: 2017-2027, 2022.
29. Chen L, Yang R, Qiao W, Zhang W, Chen J, Mao L, Goltzman D and Miao D: 1,25-Dihydroxyvitamin D exerts an antiaging role by activation of Nrf2-antioxidant signaling and inactivation of p16/p53-senescence signaling. Aging Cell 18: e12951, 2019.
30. Lee JJ, Ng SC, Hsu JY, Liu H, Chen CJ, Huang CY and Kuo WW: Galangin reverses H_2O_2-induced dermal fibroblast senescence via SIRT1-PGC-1α/Nrf2 signaling. Int J Mol Sci 23: 1387, 2022.
31. Kumar N, Reddi S, Devi S, Mada SB, Kapila R and Kapila S: Nrf2 dependent antiaging effect of milk-derived bioactive peptide in old fibroblasts. J Cell Biochem 120: 9677-9691, 2019.